Local Rational Modeling for Identification Beyond the Nyquist Frequency Applied to a Prototype Wafer Stage

van Haren, Max; Blanken, Lennart; Classens, Koen; Oomen, Tom

DOI
10.1109/TCST.2025.3568550

Publication date
2025

Document Version
Final published version

Published in
IEEE Transactions on Control Systems Technology

Local Rational Modeling for Identification Beyond the Nyquist Frequency: Applied to a Prototype Wafer Stage

Max van Haren, Lennart Blanken, Koen Classens, *Graduate Student Member, IEEE*, and Tom Oomen, *Senior Member, IEEE*

***Abstract*—Fast-rate models are essential for control design, specifically to address intersample behavior. The aim of this article is to develop a frequency-domain nonparametric identification technique to estimate fast-rate models of systems that have relevant dynamics and allow for actuation above the Nyquist frequency of a slow-rate output. Examples of such systems include vision-in-the-loop systems. Through local rational models over multiple frequency bands, aliased components are effectively disentangled, particularly for lightly damped systems. The developed technique accurately determines nonparametric fast-rate models of systems with slow-rate outputs, all within a single identification experiment. Finally, the effectiveness of the technique is demonstrated through experiments conducted on a prototype wafer stage used for semiconductor manufacturing.**

***Index Terms*—Frequency response function (FRF), local parametric modeling, sampled-data systems, system identification.**

I. Introduction

SYSTEMS with actuation and dynamics that exceed the Nyquist frequency of the sensor are becoming increasingly more common in mechatronics, for example, in hard disk drives [1] and vision-in-the-loop applications [2]. The Nyquist-Shannon sampling theorem [3] implies that these systems are usually identified up to the Nyquist frequency of the slow-rate sensor. On the other hand, fast-rate models are often necessary for tasks such as control design [1], [4] and intersample performance assessment [5].

Received 14 March 2025; accepted 6 May 2025. Date of publication 22 May 2025; date of current version 23 October 2025. This work was supported in part by VIDI through Netherlands Organization for Scientific Research (NWO) under Project 15698 and in part by the ECSEL Joint Undertaking through European Union Horizon 2020 Research and Innovation Programme under Grant 101007311 (IMOCO4.E). Recommended by Associate Editor J. T. Gravdahl. *(Corresponding author: Max van Haren.)*

Max van Haren and Koen Classens are with the Control Systems Technology Section, Department of Mechanical Engineering, Eindhoven University of Technology, 5600 MB Eindhoven, The Netherlands (e-mail: m.j.v.haren@tue.nl; k.h.j.classens@tue.nl).

Lennart Blanken is with Sioux Technologies, 5633 AA Eindhoven, The Netherlands, and also with the Control Systems Technology Section, Department of Mechanical Engineering, Eindhoven University of Technology, 5600 MB Eindhoven, The Netherlands (e-mail: l.l.g.blanken@tue.nl).

Tom Oomen is with the Control Systems Technology Section, Department of Mechanical Engineering, Eindhoven University of Technology, 5600 MB Eindhoven, The Netherlands, and also with Delft Center for Systems and Control, Delft University of Technology, 2628 CD Delft, The Netherlands (e-mail: t.a.e.oomen@tue.nl).

Digital Object Identifier 10.1109/TCST.2025.3568550

Control design and performance evaluation of linear time-invariant (LTI) systems often involves nonparametric frequency-domain models. Techniques such as manual loop-shaping [6] and parametric system identification [7] commonly employ nonparametric frequency-domain models. Frequency response functions (FRFs) are widely used to represent systems in the frequency domain, and can be directly identified from input-output data, providing a quick, accurate, and cost-effective solution [8], [9]. Furthermore, FRFs enable the direct analysis of stability, performance, and robustness [10].

Recently, more advanced FRF identification techniques have been developed, including the local polynomial modeling (LPM) method [11], [12]. LPM essentially estimates a polynomial model in a local frequency window using a least-squares cost function. LPM generally leads to an improved estimate of the FRF, which is mainly enabled by the concurrent estimation and suppression of transient contributions. Following the LPM method, the local rational modeling (LRM) technique has been developed. Unlike LPM, LRM estimates a rational model within a local frequency window [13], [14], which is shown to be more effective for lightly damped resonant dynamics [15].

Irrespective of the identification approach, identifying fast-rate models using slow-rate outputs is challenging due to aliasing. Aliasing occurs when a signal is sampled at a rate that is insufficient to capture the fast-rate dynamics of a system, preventing the unique recovery of the associated fast-rate model [16].

Substantial research has been done on the identification of fast-rate models using slow-rate outputs, with a primary focus on continuous-time and multirate parametric system identification. First, continuous-time system identification identifies a continuous-time parametric model using input-output data [17]. These methods typically constrain the input signal, such as zero-order hold or band-limited signals [18], [19]. Second, parametric identification of fast-rate models using multirate data has been developed, including impulse response [20], ARX [21], [22], and output-error [23] model estimation. Furthermore, state-space models of multirate systems are generally identified using the lifting technique [24], [25]. All these methods focus on parametric models, in addition, require intersample assumptions on the input signal, and do not take full advantage of fast-rate inputs, thereby failing to disentangle aliased components.

A recent study introduced a novel nonparametric approach for identifying fast-rate models beyond the Nyquist of a slow-rate output, where aliased contributions are disentangled by assuming locally smooth behavior of the FRF [26]. The resulting method identifies FRFs in a single identification experiment beyond the Nyquist frequency. However, [26] models the FRF locally using a finite-order polynomial, which is not capable of modeling resonant behavior accurately [13].

Although methods for identification beyond the Nyquist frequency of slow-rate outputs have been developed, there is a need for an efficient and systematic methodology for single-experiment FRF identification of fast-rate models, which disentangles aliased components with broadband input signals. In this article, fast-rate models are identified with broadband excitation signals and slow-rate outputs, where, through the use of local rational models over multiple frequency bands, aliased components are disentangled from each other. The use of local models is at the foundation of modern FRF identification for LTI single-rate systems, such as the LPM and LRM techniques. In fact, both LPM and LRM for LTI single-rate systems are recovered as a special case of the developed framework. The key contributions of this article include the following.

- C1 Formulation of a nonconvex optimization for FRF identification beyond the Nyquist frequency based on LRM across multiple frequency bands to disentangle aliased components.
- C2 A solution approach through an appropriately weighted linear least-squares criterion, which has a closed-form minimizer. Furthermore, the accuracy of the weighted cost is improved through the use of iterative reweighted solutions.
- C3 Validation of the developed framework on an experimental prototype wafer stage used for semiconductor manufacturing.

The approach in [26] is recovered as a special case of the developed framework. While the method in this article is applicable to all systems, including highly-damped systems, it is particularly suitable for systems with lightly damped resonant dynamics in contrast to [26]. This is validated using experimental data of a lightly damped prototype wafer stage.

Notations: Fast-rate signals are denoted by subscript h, and slow-rate signals with subscript l, which have been downsampled by a factor $F \in \mathbb{Z}_{>0}$, with integers $\mathbb{Z}$. Fast- and slow-rate signals consist of, respectively, N and $M = (N/F)$ data points. The N- and M-point discrete Fourier transform (DFT) for finite-time fast- and slow-rate signals is given by

$$\begin{aligned} X_h(k) &= \sum_{n=0}^{N-1} x_h(n)\, e^{-j\omega_k n T_h}, \\ X_l(k) &= \sum_{m=0}^{M-1} x_l(m)\, e^{-j\omega_k m T_l} \\ &= \sum_{n=0}^{M-1} x_h(nF)\, e^{-j\omega_k n T_l}, \end{aligned} \tag{1}$$

with, respectively, sampling times T_h and $T_l = FT_h$, discrete-time indices for fast-rate signals $n \in \mathbb{Z}_{[0,N-1]}$ and slow-rate signals $m \in \mathbb{Z}_{[0,M-1]}$, and frequency bin $k \in \mathbb{Z}_{[0,N-1]}$, which relates to the frequency grid

$$\omega_k = \frac{2\pi k}{NT_h} = \frac{2\pi k}{MT_l}. \tag{2}$$

The complex conjugate of A is denoted as $\overline{A}$ and the complex conjugate transpose as A^H. The expected value of a random variable X is given by $\mathbb{E}\{X\}$.

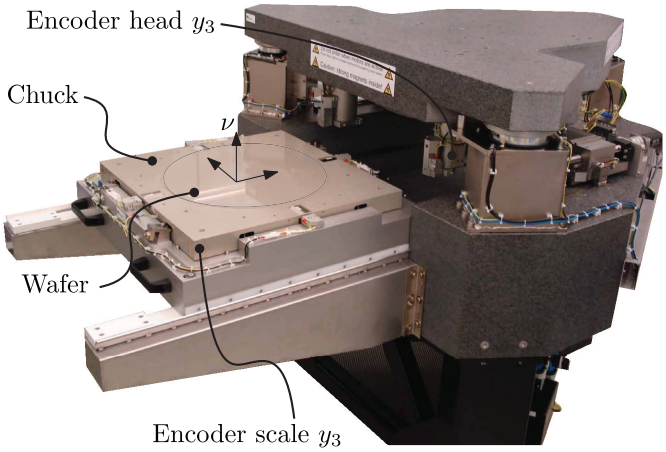

Fig. 1. Photograph of experimental setup, containing the wafer stage.

II. Problem Formulation

In this section, a motivating application and the identification setting are shown for identification beyond the Nyquist frequency of slow-rate outputs. Finally, the problem treated in this article is defined.

A. Motivating Application

The problem addressed in this article is directly motivated by the considered prototype wafer stage in Fig. 1, which is used in semiconductor manufacturing. Specifically, the over-actuated test rig (OAT) is a prime example of a mechatronic system with a slow-rate output.

The objective of the OAT is to accurately control the vertical position ν of the point of interest on the wafer, which is the point on the wafer during lithographic exposure. Directly measuring the vertical displacement of the point of interest on the wafer is not possible using linear encoders. The chuck of the OAT has internal lightly damped structural modes, and hence, measuring the vertical displacement on the outside of the chuck does not coincide with the vertical displacement at the point of interest on the wafer [27], [28]. Therefore, an external capacitive sensor that directly measures the point of interest is employed, as denoted by the scanning sensor in Fig. 2. The external capacitive sensor is sampled at a reduced sampling rate compared to the actuators.

The OAT, characterized by its slow-rate sensor and lightly damped resonant behavior, directly motivates the need for rational identification techniques beyond the Nyquist frequency.

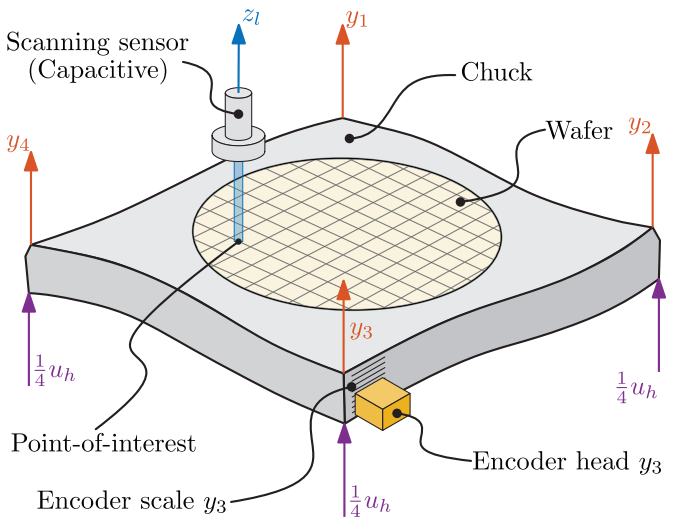

Fig. 2. Schematic overview of the experimental setup, where the fast-rate input u_h is distributed over the four corners of the chuck. The outputs used for feedback y_i $\forall i \in \{1,2,3,4\}$ are measured using encoder scales and heads, which is schematically depicted for y_3. The performance output z_l is measured using an additional capacitive scanning sensor, which is suspended less than 1 mm above the wafer and sampled at a reduced sampling rate.

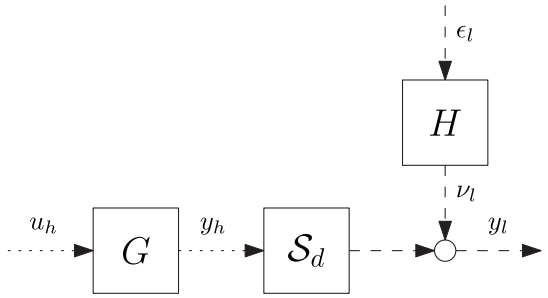

Fig. 3. Open-loop identification setting considered. The fast-rate system G with fast-rate input u_h and output y_h have sampling times T_h. The slow-rate output y_l is downsampled and disturbed with measurement noise, i.e., $y_l = \mathcal{S}_d y_h + H\epsilon_l$, and has sampling time $T_l = FT_h$.

B. Identification Setting

The goal is to identify a nonparametric FRF of fast-rate system G using slow-rate outputs y_l and fast-rate inputs u_h, as shown in Fig. 3. The set of systems G, which is considered, is described by the LTI discrete-time rational transfer function

$$G(q) = \frac{B(q)}{A(q)} = \frac{\sum_{i=0}^{n_b} b_i q^{-i}}{\sum_{i=0}^{n_a} a_i q^{-i}}, \tag{3}$$

where q^{-1} denotes the lag operator $q^{-1}x(n) = x(n-1)$. The fast-rate output y_h of system G under input u_h is given by

$$y_h(n) = G(q)\,u_h(n) + t(n), \tag{4}$$

with transient contribution $t(n)$, which includes leakage and occurs due to finite-length signals [11], [14]. Taking the DFT on both sides of (4) results in

$$Y_h(k) = G(\Omega_k)\,U_h(k) + T(\Omega_k), \tag{5}$$

with generalized frequency variable $\Omega_k = e^{-j\omega_k T_h}$ for discrete-time systems and transient contribution $T(\Omega_k)$. Since G is assumed to be LTI and described according to (3), the fast-rate output $Y_h(k)$ is only influenced by a single frequency of $U_h(k)$, commonly denoted by the frequency-separation principle. The fast-rate output is downsampled, as shown in Fig. 3, into

$$Y_l(k) = \mathcal{S}_d Y_h(k) + V_l(k), \tag{6}$$

with noise $V_l(k) = H(\Omega_k)E(k)$, where $E(k)$ is zero-mean independent and identically distributed noise. The transient of the noise system H is typically neglected since it is negligible compared to its steady-state response $H\epsilon_l$ [8, Sec. 6.7.3.4]. The downsampling operation in (6) is equal to the time-domain operation $y_l(m) = y_h(nF) + v_l(m)$. The DFT of the slow-rate output is found by expanding the downsampling operation in (6) [29], i.e.,

$$Y_l(k) = \frac{1}{F}\sum_{f=0}^{F-1} Y_h(k+fM) + V_l(k). \tag{7}$$

By substituting the fast-rate output from (5) into (7), the slow-rate output results in

$$Y_l(k) = \frac{1}{F}\sum_{f=0}^{F-1}\left(G\left(\Omega_{k+fM}\right)U_h(k+fM) + T_G\left(\Omega_{k+fM}\right)\right) + V_l(k). \tag{8}$$

C. Problem Definition

The downsampler results in the DFT of the output (8) being affected by F contributions from the system $G(\Omega_{k+fM})$ and transient $T(\Omega_{k+fM})$. Therefore, the fast-rate FRF $G(\Omega_k)$ can, in general, not be uniquely identified beyond the Nyquist frequency of the slow-rate using fast-rate inputs u_h.

The problem considered is given as follows. Given fast-rate inputs u_h and slow-rate outputs y_l from the system $\mathcal{S}_d G$ in Fig. 3, identify a fast-rate FRF $\widehat{G}(\Omega_k)$ for the frequencies Ω_k $\forall k \in \mathbb{Z}_{[0,N-1]}$, i.e., up to the fast sampling frequency $f_h = (1/T_h)$. Throughout the article, requirements on the fast-rate input signal u_h are investigated as well.

III. LRM Beyond the Nyquist Frequency

In this section, local rational models across multiple frequency bands are developed to identify fast-rate models beyond the Nyquist frequency of a slow-rate sensor under broadband excitation, leading to contribution C1.

The rational description of G in (3) motivates parameterizing a model within the local frequency window $r \in \mathbb{Z}_{[-n_w,n_w]}$, with $2n_w+1$ being the window size, as

$$\widehat{G}\left(\Omega_{k+r+fM}\right) = \frac{n\left(\Omega_{k+r+fM}\right)}{d\left(\Omega_{k+r+fM}\right)} \quad \forall f \in \mathbb{Z}_{[0,F-1]}, \tag{9}$$

where each (k,r,f) results in the independently parameterized local models

$$n\left(\Omega_{k+r+fM}\right) = \widehat{G}\left(\Omega_{k+fM}\right) + \sum_{s=1}^{R_n} n_s(k+fM)\,r^s,$$
$$d\left(\Omega_{k+r+fM}\right) = 1 + \sum_{s=1}^{R_d} d_s(k+fM)\,r^s. \tag{10}$$

Similarly, the transient T is parameterized as

$$\widehat{T}\left(\Omega_{k+r+fM}\right) = \frac{m\left(\Omega_{k+r}\right)}{d\left(\Omega_{k+r+fM}\right)}, \tag{11}$$

where the same denominator is used as for the system G since G and T share the same poles [13]. Solely, the contribution of the transient in the slow-rate output Y_l is of interest, and hence, the numerator of the transient $m(\Omega_{k+r})$ is modeled at the slow-rate and independently of the frequency band f, i.e.,

$$m\left(\Omega_{k+r}\right) = \widehat{T}\left(\Omega_k\right) + \sum_{s=1}^{R_m} m_s\left(k\right) r^s, \tag{12}$$

which allows to suppress the transient contribution. The polynomial degrees R_n, R_d, and R_m influence how accurately the local model can approximate the system's FRF. Higher values allow for more flexibility in the approximated FRF, enabling the model to capture high-order effects in the frequency response such as lightly damped resonances.

The slow-rate output in window $k+r$ is estimated using the local models of the system and transient $\widehat{G}$ and $\widehat{T}$, given the input signal $U(k+r)$, as

$$\widehat{Y}_l\left(k+r\right) = \frac{1}{F}\sum_{f=0}^{F-1}\left(\widehat{G}\left(\Omega_{k+r+fM}\right) U\left(k+r+fM\right) + \widehat{T}\left(\Omega_{k+r+fM}\right)\right). \tag{13}$$

The local parameterization of the system and transient in (9) and (11) leads to the estimated output

$$\begin{aligned}\widehat{Y}_l\left(k+r\right) = {} & \frac{1}{F}\sum_{f=0}^{F-1}\frac{\widehat{T}\left(\Omega_k\right) + \sum_{s=1}^{R_m} m_s\left(k\right) r^s}{1+\sum_{s=1}^{R_d} d_s\left(k+fM\right) r^s} \\ & + \frac{1}{F}\sum_{f=0}^{F-1}\frac{\widehat{G}\left(\Omega_{k+fM}\right) + \sum_{s=1}^{R_n} n_s\left(k+fM\right) r^s}{1+\sum_{s=1}^{R_d} d_s\left(k+fM\right) r^s} \\ & \times U\left(k+r+fM\right).\end{aligned} \tag{14}$$

The parameters are gathered in a vector $\widehat{\Theta}(k) \in \mathbb{C}^{1\times(F(R_n+1+R_d)+R_m+1)}$, i.e., (15), as shown at the bottom of the page, where

$$\begin{aligned}\theta_{\widehat{G}} &= \frac{1}{F}\begin{bmatrix}\widehat{G}\left(\Omega_k\right) & \widehat{G}\left(\Omega_{k+M}\right) & \cdots & \widehat{G}\left(\Omega_{k+(F-1)M}\right)\end{bmatrix}, \\ \theta_N &= \frac{1}{F}\begin{bmatrix}\theta_{n_1} & \theta_{n_2} & \cdots & \theta_{n_{R_n}}\end{bmatrix}, \\ \theta_D &= \begin{bmatrix}\theta_{d_1} & \theta_{d_2} & \cdots & \theta_{d_{R_d}}\end{bmatrix},\end{aligned} \tag{16}$$

and

$$\begin{aligned}\theta_{n_i} &= \begin{bmatrix}n_i\left(k\right) & n_i\left(k+M\right) & \cdots & n_i\left(k+(F-1)M\right)\end{bmatrix}, \\ \theta_{d_i} &= \begin{bmatrix}d_i\left(k\right) & d_i\left(k+M\right) & \cdots & d_i\left(k+(F-1)M\right)\end{bmatrix}.\end{aligned} \tag{17}$$

The decision parameters $\widehat{\Theta}$ are determined by optimizing an objective function, i.e.,

$$\min_{\widehat{\Theta}(k)} J\left(\widehat{\Theta}\left(k\right)\right). \tag{18}$$

As an objective function, the least-squares residual between estimated and measured outputs Y_l within the local frequency window $k+r$ is given by

$$J_{\mathrm{LS}}\left(\widehat{\Theta}\left(k\right)\right) = \sum_{r=-n_w}^{n_w}\left\|Y_l\left(k+r\right) - \widehat{Y}_l\left(k+r,\widehat{\Theta}\left(k\right)\right)\right\|_2^2. \tag{19}$$

Remark 1: LRM for single-rate LTI systems with a nonlinear cost function [14] is recovered as a special case of the framework by setting $F = 1$. Furthermore, if $F = 1$ and $d(\Omega_{k+r}) = 1$, i.e., $R_d = 0$, LPM for single-rate LTI systems [11], [12] is recovered.

Optimizing the cost function (19) is challenging because 1) it involves a summation due to the downsampling operation and 2) the system and transient are rationally parameterized, as shown in (14). Given the rational model structure and the downsampling operation, the cost function in (19) is nonlinear with respect to the parameters $\widehat{\Theta}(k)$. As a result, it is generally nonconvex and does not have a closed-form solution.

IV. FRF Identification Beyond the Nyquist Frequency With Local Rational Models

In this section, a solution approach for unique and convex identification of local rational models beyond the Nyquist frequency is presented, leading to contribution C2. The key idea is to appropriately weight the nonlinear cost (19), leading to a linear least-squares criterion. The unique existence of the closed-form solution is guaranteed through design conditions on the input and local models. In addition, the closed-form solution enables to approximate the variance of the FRF. Subsequently, the accuracy of the weighted cost is improved through the use of iterative reweighted solution methods. Finally, the developed approach is summarized in a procedure.

A. Linear Least-Squares for LRM Beyond the Nyquist Frequency

By appropriately weighting the nonlinear cost function (19), a linear least-squares criterion is obtained, as shown in Lemma 1.

Lemma 1: By multiplying the residual $Y_l(k+r) - \widehat{Y}(k+r,\widehat{\Theta}(k))$ in (19) with

$$e\left(\Omega_{k+r}\right) = 1 + \sum_{s=1}^{R_e} e_s\left(k\right) r^s \equiv \prod_{f=0}^{F-1} d\left(\Omega_{k+r+fM}\right), \tag{20}$$

resulting in the linear least-squares criterion

$$\begin{aligned}J_W\left(\widetilde{\Theta}\left(k\right)\right) &= \sum_{r=-n_w}^{n_w}\left\|\left(1+\sum_{s=1}^{R_e} e_s\left(k\right) r^s\right)\right. \\ &\quad \left.\cdot\left(Y_l\left(k+r\right) - \widehat{Y}_l\left(k+r,\widehat{\Theta}\left(k\right)\right)\right)\right\|_2^2 \\ &= \sum_{r=-n_w}^{n_w}\left\|Y_l\left(k+r\right) - \widetilde{\Theta}\left(k\right) K\left(k+r\right)\right\|_2^2,\end{aligned} \tag{21}$$

$$\widehat{\Theta}\left(k\right) = \begin{bmatrix}\theta_{\widehat{G}} & \theta_N & \widehat{T}\left(\Omega_k\right) & m_1\left(k\right) & \cdots & m_{R_m}\left(k\right) & \theta_D\end{bmatrix}, \tag{15}$$

where $K(k+r)$ is the regressor vector of the least-squares problem and will be defined in (28).

Proof: By expressing the sum (14) as a single fraction, and substituting $\prod_{f=0}^{F-1} d(\Omega_{k+r+fM}) = e(\Omega_{k+r})$, the estimated output is (22), as shown at the bottom of the page,with polynomial coefficients $g_s(k+fM)$, $t_s(k) \in \mathbb{C}$ and

$$R_g = R_n + R_d\,(F-1)\,, R_t = R_m + R_d\,(F-1)\,, R_e = R_d F \tag{23}$$

result in the same model as in (9) and (11). Furthermore, the numerator polynomials g_s and t_s are obtained by multiplying $n_s(\Omega_{k+r+iM})$ and $m_s(\Omega_{k+r+iM})$ from (9) and (11) with all $d(\Omega_{k+r+fM})\ \forall f \neq i$, i.e.,

$$\left(\widehat{G}\left(\Omega_{k+iM}\right) + \sum_{s=1}^{R_n} n_s\left(k+iM\right) r^s\right) \prod_{f\in\mathbb{Z}_{[0,F-1]\setminus i}} d\left(\Omega_{k+r+fM}\right) r^s$$
$$\equiv \widehat{G}\left(\Omega_{k+iM}\right) + \sum_{s=1}^{R_g} g_s\left(k+iM\right) r^s, \tag{24}$$

$$\left(\widehat{T}\left(\Omega_k\right) + \sum_{s=1}^{R_m} m_s\left(k\right) r^s\right) \prod_{f\in\mathbb{Z}_{[0,F-1]\setminus i}} d\left(\Omega_{k+r+fM}\right) r^s$$
$$\equiv \widehat{T}\left(\Omega_k\right) + \sum_{s=1}^{R_t} t_s\left(k\right) r^s. \tag{25}$$

Then, by substituting (22) in the residual $Y_l(k+r) - \widehat{Y}(k+r, \widetilde{\Theta}(k))$ and multiplying with $e(\Omega_{k+r})$ from (20), the linear least-squares criterion (21) is obtained.■

The capability of the local model to approximate the system's FRF is determined by R_n, R_d, and R_m, which, together with F, determines appropriate polynomial degrees R_g, R_t, and R_e using (23).

Remark 2: LRM for single-rate LTI systems in the sense of [13] is recovered by setting $F = 1$.

The linear least-squares criterion (21), with output (22) and local models (20), (24), and (25), is formulated using the parameter row vector $\widetilde{\Theta}(k) \in \mathbb{C}^{1\times((R_g+1)F+R_t+1+R_e)}$, i.e., (26), as shown at the bottom of the page,with $\theta_{\widehat{G}}$ from (16) and (27), as shown at the bottom of the page. The input matrix $K(k+r)$ in (21) is given by

$$K\left(k+r\right) = \begin{bmatrix} K_1\left(r, R_g\right) \otimes \underline{U}\left(k+r\right) \\ K_1\left(r, R_t\right) \\ -K_2\left(r, R_d F\right) Y_l\left(k+r\right) \end{bmatrix}, \tag{28}$$

with the Kronecker product $\otimes$, $K_1(r,R) = \left[1\ r\ \cdots\ r^R\right]^\top$, $K_2(r,R) = \left[r\ \cdots\ r^R\right]^\top$, and the input vector

$$\underline{U}\left(k+r\right) = \begin{bmatrix} U\left(k+r\right) \\ U\left(k+r+M\right) \\ \vdots \\ U\left(k+r+\left(F-1\right)M\right) \end{bmatrix}. \tag{29}$$

The linear least-squares criterion (21) resolves the nonlinear optimization challenges in Section III with its closed-form minimizer, which is discussed next.

B. Closed-Form Minimizer for LRM Beyond the Nyquist Frequency

In this section, a closed-form minimizer to the linear least-squares criterion (21) is determined. The summation in (21) is removed by gathering the data in the window r as

$$J_W\left(\widetilde{\Theta}\left(k\right)\right) = \left\| Y_{l,n_w} - \widetilde{\Theta}\left(k\right) K_{n_w} \right\|_2^2, \tag{30}$$

where $K_{n_w} \in \mathbb{C}^{((R_g+1)F+R_t+1+R_e)\times(2n_w+1)}$ and $Y_{l,n_w} \in \mathbb{C}^{1\times(2n_w+1)}$ are constructed as (31), as shown at the bottom of the page.The minimizer to the cost function (30) leads to a least-squares closed-form solution for LRM beyond the Nyquist frequency, that is,

$$\widetilde{\Theta}\left(k\right) = Y_{l,n_w} K_{n_w}^H \left(K_{n_w} K_{n_w}^H\right)^{-1}. \tag{32}$$

Remark 3: The matrix inversion in (32) can be numerically unstable, especially for ill-conditioned problems. In practical implementations, numerically stable alternatives such as the singular-value decomposition [8, Sec. 7.2.2.5] are recommended.

$$\widehat{Y}_l\left(k+r, \widetilde{\Theta}\left(k\right)\right) = \frac{1}{F}\frac{\widehat{T}\left(\Omega_k\right) + \sum_{s=1}^{R_t} t_s\left(k\right) r^s}{1 + \sum_{s=1}^{R_e} e_s\left(k\right) r^s} + \frac{1}{F}\frac{\sum_{f=0}^{F-1}\left(\left(\widehat{G}\left(\Omega_{k+fM}\right) + \sum_{s=1}^{R_g} g_s\left(k+fM\right) r^s\right) U\left(k+r+fM\right)\right)}{1 + \sum_{s=1}^{R_e} e_s\left(k\right) r^s} \tag{22}$$

$$\widetilde{\Theta}\left(k\right) = \begin{bmatrix} \theta_{\widehat{G}} & \theta_g & \widehat{T}\left(\Omega_k\right) & t_1\left(k\right) & \cdots & t_{R_t}\left(k\right) & \theta_e \end{bmatrix}, \tag{26}$$

$$\theta_g = \frac{1}{F}\begin{bmatrix} g_1\left(k\right) & g_1\left(k+M\right) & \cdots & \cdots & g_{R_g}\left(k+\left(F-1\right)M\right) \end{bmatrix}$$
$$\theta_e = \begin{bmatrix} e_1\left(k\right) & e_2\left(k\right) & \cdots & e_{R_e}\left(k\right) \end{bmatrix}. \tag{27}$$

$$K_{n_w} = \begin{bmatrix} K\left(k-n_w\right) & K\left(k-n_w+1\right) & \cdots & K\left(k+n_w\right) \end{bmatrix},$$
$$Y_{l,n_w} = \begin{bmatrix} Y_l\left(k-n_w\right) & Y_l\left(k-n_w+1\right) & \cdots & Y_l\left(k+n_w\right) \end{bmatrix}. \tag{31}$$

The fast-rate models at the frequency bands $k + fM\ \forall f \in \mathbb{Z}_{[0,F-1]}$ are jointly estimated by

$$\begin{bmatrix} \widehat{G}(\Omega_k) \\ \widehat{G}(\Omega_{k+M}) \\ \vdots \\ \widehat{G}(\Omega_{k+(F-1)M}) \end{bmatrix}^{\top} = F\widetilde{\Theta}(k)\begin{bmatrix} I_F & 0_{F\times R_g F+R_t+1+R_e} \end{bmatrix}^{\top}, \quad \forall k \in \mathbb{Z}_{[0,M-1]}, \tag{33}$$

and similarly for the transient $\widehat{T}(\Omega_k)$.

Necessary conditions for the uniqueness of the closed-form solution (32) to linear least-squares criterion J_W in (21) are given by

$$2n_w + 1 \geq \left(R_g + 1\right) F + R_t + 1 + R_e, \tag{34a}$$

$$2n_w + 1 \leq M, \tag{34b}$$

$$|U(k + r_1 + iM) - U(k + r_2 + jM)| \neq 0, \quad \forall r_1, r_2 \in \mathbb{Z}_{[-n_w,n_w]} \quad \forall i, j \in \mathbb{Z}_{[0,F-1]}, \quad \forall r_1 + iM \neq r_2 + jM. \tag{34c}$$

In practice, it is observed from experimental data that the conditions (34) generally lead to the existence of unique solutions (32). The conditions (34) are to be interpreted as design criteria on the input and local models as follows.

1) For each frequency bin k, the amount of estimated parameters $(R_g + 1)F + R_t + 1 + R_e$ in $\widetilde{\Theta}$ should be less than the number of data points $2n_w + 1$, leading to (34a). This intuitively explains how the local models with $(R_g+1)F+R_t+1+R_e$ parameters $\widetilde{\Theta}$ in (32) enable disentangling F aliased contributions through the use of $2n_w + 1$ outputs $Y_l(k + r)$.
2) The window size $2n_w+1$ should not exceed the amount of data points M in Y_{l,n_w}, leading to (34b).
3) K_{n_w} is full (row) rank if all inputs in the local and aliased windows $\underline{U}(k + r)$ are sufficiently "rough," which is formalized for a single local window in [11]. For (32), this requires that the spectral difference $|U(k+r_1+iM)-U(k+r_2+iM)|$ in (34c) does not vanish. This is satisfied with high probability for random-phase multisines [8], [11], except for rare degenerate cases. In addition, the spectral difference condition can be verified before the identification experiment, enabling the generation of new realizations until a sufficiently rough signal is obtained.

Remark 4: To prevent the Vandermonde structure in the matrix K_{n_w} from becoming ill-conditioned, R_g, R_t, and R_e should not be chosen excessively high. Alternatively, the numerical conditioning can be improved according to [14].

Remark 5: Identification of FRFs beyond the Nyquist frequency using slow-rate outputs with LPM [26] is a special case of the developed framework by setting $R_e = 0$ and $R_g = R_t$.

Remark 6: The windows for the left and right frequency borders are $k+r \in \mathbb{Z}_{[0,2n_w]}\ \forall k \leq n_w$ and $k+r \in \mathbb{Z}_{[M-2n_w,M]}\ \forall k > M - n_w$ similar to [8, Sec. 7.2.2.6].

In addition, the closed-form solution enables approximating the variance, which is presented in Lemma 2.

Lemma 2: Let the system and transient be modeled using (9) and (11). Then, the estimated variance of the FRF $\widehat{G}(\Omega_k)$, determined with (33), is given by

$$\operatorname{var}\left(\widehat{G}(\Omega_k)\right) \approx F^2\overline{S^H S}\,\widehat{C}_v(k) \quad \forall k \in \mathbb{Z}_{[0,M-1]}, \tag{35}$$

which is an estimate of the true variance of the identified FRF

$$\operatorname{var}\left(\widehat{G}(\Omega_k)\right) = F^2\overline{\mathbb{E}\left(S^H S\right)}C_v(k) + F^2 O_{\text{int,H}}\left(\frac{n_w^0}{M}\right), \tag{36}$$

with variance of the noise C_v and its estimate $\widehat{C}_v$, noise interpolation error $O_{\text{int,H}}$ [8], and

$$S = K_{n_w}^H\left(K_{n_w}K_{n_w}^H\right)^{-1}\begin{bmatrix} 1 & 0_{1\times F(R_g+1)+R_t+R_e} \end{bmatrix}, \tag{37}$$

and similarly for the FRF at the frequency bands $k+fM\ \forall f \in \mathbb{Z}_{[1,F-1]}$.

Proof: The results of [8, Appendix 7.E] and [26] apply, respectively, for $F = 1$, and $R_e = 0$ and $R_g = R_t$. Furthermore, for arbitrary F, R_e, R_g, and R_t, the system output for window n_w for the local models in (9) and (11) is given by

$$Y_{l,n_w} = \widetilde{\Theta}_0(k)\,K_{n_w} + V_{l,n_w}, \tag{38}$$

where $\widetilde{\Theta}_0(k)$ has the same structure as $\widetilde{\Theta}(k)$ in (26) but containing the true parameters of the system. Rewriting (38), multiplying by S, and combining with (32) result in

$$\begin{aligned} \left(Y_{l,n_w} - \widetilde{\Theta}_0(k)\,K_{n_w}\right)S &= V_{n_w}S, \\ \widetilde{\Theta}(k)\begin{bmatrix} 1 & 0 \end{bmatrix}^{\top} - \widetilde{\Theta}_0(k)\begin{bmatrix} 1 & 0 \end{bmatrix}^{\top} &= V_{n_w}S, \\ \frac{1}{F}\widehat{G}(\Omega_k) - \frac{1}{F}G(\Omega_k) &= V_{n_w}S, \\ \widehat{G}(\Omega_k) &= G(\Omega_k) + FV_{n_w}S, \end{aligned} \tag{39}$$

where the variance is calculated as $\operatorname{var}(\widehat{G}(\Omega_k)) = \mathbb{E}(\widehat{G}(\Omega_k)\widehat{G}^H(\Omega_k))$.■

The variance of the noise $C_v(k) = \operatorname{var}(V_l(k)) = \mathbb{E}(V_l(k)V_l^H(k))$ is estimated using the residual of the least-squares fit [8, Appendix 7.B], i.e.,

$$\widehat{C}_v(k) = \frac{1}{q}\left(Y_{l,n_w} - \widetilde{\Theta}(k)\,K_{n_w}\right)\left(Y_{l,n_w} - \widetilde{\Theta}(k)\,K_{n_w}\right)^H, \tag{40}$$

with degrees of freedom $q = 2n_w+1-((R_g+1)F+R_t+1+R_e)$.

Remark 7: The polynomial degrees R_g, R_t, and R_e and the window size n_w should be appropriately chosen for the system at hand while satisfying conditions (34a) and (34b) and can be tuned to minimize the estimated variance (35). Since there are aliased dynamics, it is recommended to use slightly higher degrees than 2, which is recommended in [8, Sec. 7.2.2]. Alternatively, the degrees could be optimized using a heuristic, as shown in [30], which is not the scope of this article.

The linear least-squares criterion (21) is obtained by appropriately weighting the nonlinear cost function in (19), which has closed-form solution (32). Generally, this method is effective, especially for practical applications [14], [31]. In addition, iterative reweighted solutions further enhance the accuracy of weighted linear least-squares.

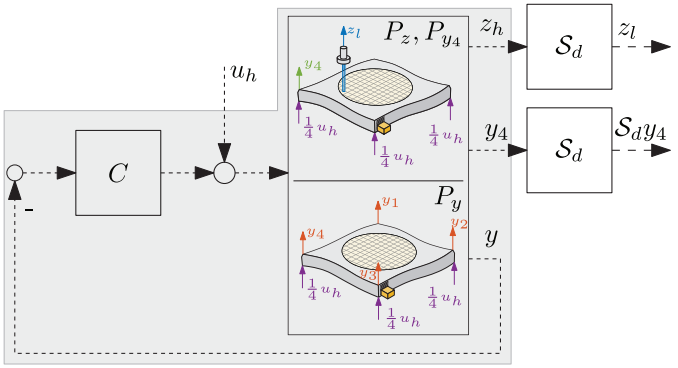

Fig. 4. Experimental feedback scheme used, where the equivalent systems in (47) are to be identified.

C. Iterative Reweighted Solutions

The accuracy of the weighted least-squares criterion (21) is improved through iterative reweighted solutions. Both the Sanathanan-Koerner (SK) and Levenberg-Marquardt (LM) algorithms are employed for this purpose.

1) Sanathanan-Koerner Algorithm: The SK algorithm [32] iteratively counteracts the weighting from (21) by reweighting with its inverse determined in the previous SK iteration. Hence, the iteratively minimized cost function is

$$J_{\mathrm{SK}}\left(\widetilde{\Theta}^{\langle j\rangle}(k)\right) = \sum_{r=-n_w}^{n_w} \left\| \left(1+\sum_{s=1}^{R_e} e_s^{\langle j-1\rangle}(k)\, r^s\right)^{-1} \times \left(1+\sum_{s=1}^{R_e} e_s^{\langle j\rangle}(k)\, r^s\right) \times \left(Y_l(k+r) - \widehat{Y}_l\left(k+r, \widetilde{\Theta}^{\langle j\rangle}(k)\right)\right) \right\|_2^2 \tag{41}$$

which is minimized until convergence or a stopping criterion is met. As initial guess, the closed-form solution from (32) can be used, i.e.,

$$\widetilde{\Theta}^{\langle 0\rangle}(k) = \widetilde{\Theta}(k) \quad \forall k. \tag{42}$$

Conveniently, the iterative solution is determined similar to the closed-form solution in (32), that is,

$$\widetilde{\Theta}^{\langle j\rangle}(k) = Z_{l,n_w}^{\langle j-1\rangle}\left(L_{n_w}^{\langle j-1\rangle}\right)^H \left(L_{n_w}^{\langle j-1\rangle}\left(L_{n_w}^{\langle j-1\rangle}\right)^H\right)^{-1}, \tag{43}$$

where $Z_{l,n_w}^{\langle j-1\rangle}$ and $L_{n_w}^{\langle j-1\rangle}$ are constructed similar to (31), i.e.,

$$\begin{aligned} L_{n_w}^{\langle j-1\rangle} &= \left[L^{\langle j-1\rangle}(k-n_w) \quad \cdots \quad L^{\langle j-1\rangle}(k+n_w)\right], \\ Z_{l,n_w}^{\langle j-1\rangle} &= \left[Z_l^{\langle j-1\rangle}(k-n_w) \quad \cdots \quad Z_l^{\langle j-1\rangle}(k+n_w).\right] \end{aligned} \tag{44}$$

with their components

$$\begin{aligned} Z_l^{\langle j-1\rangle}(k+r) &= \left(1+\sum_{s=1}^{R_e} e_s^{\langle j-1\rangle}(k)\, r^s\right)^{-1} Y_l(k+r), \\ L^{\langle j-1\rangle}(k+r) &= \left(1+\sum_{s=1}^{R_e} e_s^{\langle j-1\rangle}(k)\, r^s\right)^{-1} K(k+r). \end{aligned} \tag{45}$$

While the SK algorithm does not guarantee monotonic convergence, it has been successfully applied in the system identification literature with attractive convergence properties, specifically in practical situations [33]. The accuracy of the solution with respect to the original cost function is further increased via the LM algorithm.

Procedure 1 Identify Fast-Rate FRF Using Slow-Rate Outputs and Fast-Rate Broadband Inputs With Local Rational Model

1) Construct u_h, such that it satisfies the requirements of $\underline{U}$ in (34c), e.g., random-phase multisines.
2) Apply input u_h to system and record the output y_l.
3) Take the DFT of input u_h and output y_l using (1).
4) For frequency bins $k \in \mathbb{Z}_{[0,M-1]}$, determine $\widehat{G}(\Omega_{k+fM})\ \forall f \in \mathbb{Z}_{[0,F-1]}$, which can be done in the following two ways.
   a) Directly optimize the non-linear cost in (19), using a non-linear optimizer.
   b) Or, optimize the linear least-squares criterion (21).
      i) Use (31) to construct matrices K_{n_w} and Y_{l,n_w}, with measured outputs $Y_l(k+r)$ and input vectors $K(k+r)$ from (28), using $\underline{U}(k+r)$.
      ii) Compute parameter vector $\widetilde{\Theta}(k)$ from (32), and consequently the FRF $\widehat{G}(\Omega_{k+fM})\ \forall f \in \mathbb{Z}_{[0,F-1]}$ using (33).
      iii) Calculate the estimated variance of the FRF with Lemma 2.
      iv) Optional: Refine optimizer using the SK or LM algorithms, as described in Section IV-A.

2) Levenberg-Marquardt Algorithm: Second, a nonlinear optimizer can be used to optimize the original cost function (19) with parameters $\widetilde{\Theta}$, i.e.,

$$\begin{aligned} J_{\mathrm{LM}}\left(\widetilde{\Theta}(k)\right) &= J_{\mathrm{LS}}\left(\widehat{\Theta}(k)\right) \\ &= \sum_{r=-n_w}^{n_w} \left\| Y_l(k+r) - \widehat{Y}_l\left(k+r, \widetilde{\Theta}(k)\right)\right\|_2^2, \end{aligned} \tag{46}$$

where $\widehat{Y}_l(k+r, \widetilde{\Theta}(k))$ is calculated using (22). The LM algorithm, which is a damped Gauss-Newton algorithm, has been successfully applied for local modeling in [14]. Until convergence or a stopping criterion is met, the parameters are updated based on the Jacobian of the residual with respect to the parameters. As an initial guess, the closed-form solution from (32) can be used. Alternatively, the LM algorithm can be used complementary to the SK algorithm by using the result from the SK algorithm as an initial guess. The LM algorithm optimizes the original cost function, and hence, a local minimum of the original cost function is found. However, since the cost function is nonlinear, the LM algorithm does not guarantee convergence to the global minimum, and its result is strongly dependent on the initial guess.

With this in mind, it is recommended to start with solution (32) of the linear least-squares criterion (21) and perform SK iterations. Subsequently, the result of the SK algorithm serves as a good initial guess for the LM algorithm.

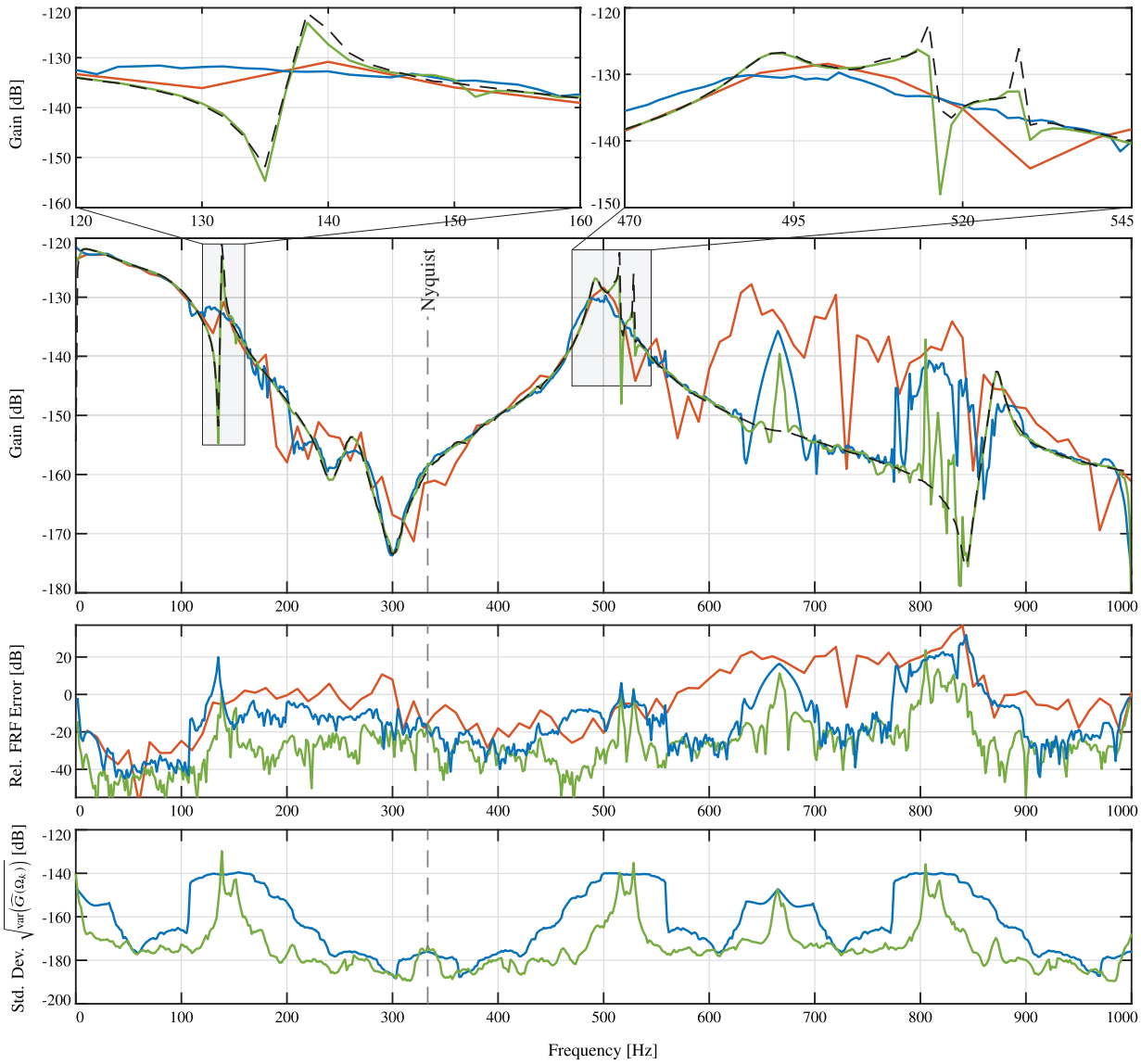

Fig. 5. Developed LRM method $\widehat{G}_{\mathrm{LRM}}(\Omega_k)$ (—) identifies the true system $G_{y_4}(\Omega_k)$ (– –) accurately, even beyond the Nyquist frequency (– –) (second row) and the lightly damped resonant dynamics (enlarged in top row). Both $\widehat{G}_{\mathrm{LPM}}(\Omega_k)$ (—) and $\widehat{G}_{\mathrm{SA}}(\Omega_k)$ (—) identify the true system $G_{y_4}(\Omega_k)$ (– –) significantly less accurately, which is confirmed by their corresponding relative FRF errors $|G_{y_4}(\Omega_k) - \widehat{G}(\Omega_k)|/|G_{y_4}(\Omega_k)|$ (third row). Estimated standard deviation of $\widehat{G}_{\mathrm{LPM}}(\Omega_k)$ (—) and $\widehat{G}_{\mathrm{LRM}}(\Omega_k)$ (—), calculated using the square root of (35), shows similar behavior as the FRF error (bottom row).

D. Procedure for LRM Beyond the Nyquist Frequency

The main results in Sections III and IV are summarized in Procedure 1.

V. Experimental Validation

In this section, the developed framework is validated on a prototype wafer stage used for semiconductor manufacturing, leading to contribution C3. The experimental setup is introduced, followed by the results. Finally, the FRF is refined using the iterative procedures from Section IV-C.

A. Experimental Setup

The experimental setup is the OAT shown in Fig. 1. The chuck is levitated and actuated by four Lorentz-type actuators on the corners of the chuck. In addition, the vertical displacement is measured at the corners of the chuck by means of four linear encoder heads and scales, and is used as inputs to an internal feedback controller as $y = (1/4)(y_1 + y_2 + y_3 + y_4)$. For the case study, the fast-rate excitation u_h is equally distributed over the four actuators and is considered a disturbance to the plant. The scanning sensor is suspended above the wafer and can be moved in the horizontal plane. The scanning sensor is positioned in the bottom left corner of the wafer, 110 mm in both directions from the center. A schematic overview of the control scheme is shown in Fig. 4.

The goal is to identify fast-rate (equivalent) models using slow-rate outputs. Specifically, FRFs are identified for the displacement of the point of interest z_h, in addition to one of the corners of the chuck y_4, i.e.,

$$G_{y_4}(\Omega_k) = P_{y_4}(\Omega_k)\left(I + C(\Omega_k)P_y(\Omega_k)\right)^{-1} : u_h \mapsto y_4,$$
$$G_z(\Omega_k) = P_z(\Omega_k)\left(I + C(\Omega_k)P_y(\Omega_k)\right)^{-1} : u_h \mapsto z_h, \quad (47)$$

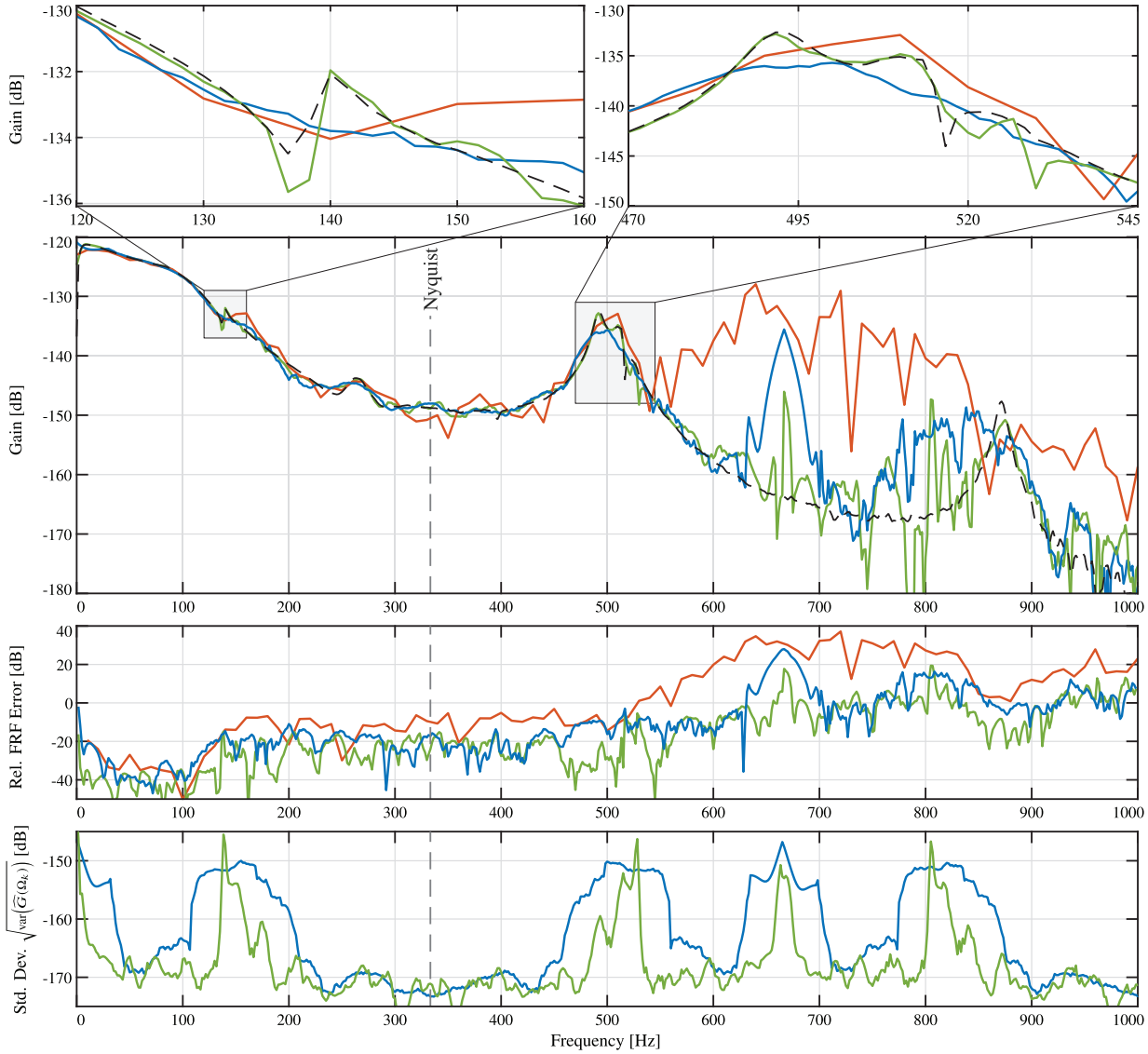

Fig. 6. Developed LRM method $\widehat{G}_{\mathrm{LRM}}(\Omega_k)$ (—) identifies the true system $G_z(\Omega_k)$ (– –) accurately, even beyond the Nyquist frequency (– –) (middle) and the lightly damped resonant dynamics (enlarged in top row). Both $\widehat{G}_{\mathrm{LPM}}(\Omega_k)$ (—) and $\widehat{G}_{\mathrm{SA}}(\Omega_k)$ (—) identify the true system $G_z(\Omega_k)$ (– –) significantly less accurate, which is confirmed by their corresponding relative FRF errors $|G_z(\Omega_k) - \widehat{G}(\Omega_k)|/|G_z(\Omega_k)|$ (third row). Estimated standard deviation of $\widehat{G}_{\mathrm{LPM}}(\Omega_k)$ (—) and $\widehat{G}_{\mathrm{LRM}}(\Omega_k)$ (—), calculated using the square root of (35), shows similar behavior as the FRF error (bottom row).

are identified using the fast-rate input u_h and slow-rate outputs $\mathcal{S}_d y_4$ and z_l.

The excitation signal is a single period of a random-phase multisine, exciting all frequencies with a flat amplitude spectrum, and having a root mean square value of 1.44 N. The signal-to-noise ratio, which is the ratio of the variance of the output z_l to the noise v_l, is estimated to be around 45 dB. Further experimental settings are shown in Table I.

The following methods are compared.

$\widehat{G}_{\mathrm{LRM}}$ The developed approach using the closed-form solution (32), with settings shown in Table I.
$\widehat{G}_{\mathrm{LPM}}$ The approach from [26], i.e., the developed approach with $R_d = R_e = 0$, $R_g \equiv R_t = 2$, and $n_w = 18$.
$\widehat{G}_{\mathrm{SA}}$ A traditional approach using spectral analysis (SA) with a Hanning window.

TABLE I
EXPERIMENTAL SETTINGS

Variable	Abbrevation	Value
Fast sampling time	T_h	0.5 ms
Slow sampling time	T_l	1.5 ms
Downsampling factor	F	3
Number of input samples	N	1200
Number of output samples	M	400
Measurement time	T_m	0.6 s
System numerator degree	R_g	4
Transient numerator degree	R_t	4
Denominator degree	R_e	7
Window size	n_w	18

The SA assumes that the DFT is periodic in the slow sampling frequency, i.e., $\widehat{Y}_h(\Omega_{k+iM}) = FY_l(\Omega_k)\ \forall i \in \mathbb{Z}$, which, in the time domain, is equivalent to interpolating z_l with zeros as $\widehat{z}_h = \begin{bmatrix} z_l(0)\ 0\ 0\ z_l(1) \cdots \end{bmatrix}^{\mathsf{T}}$ and similarly for y_4. SA averages

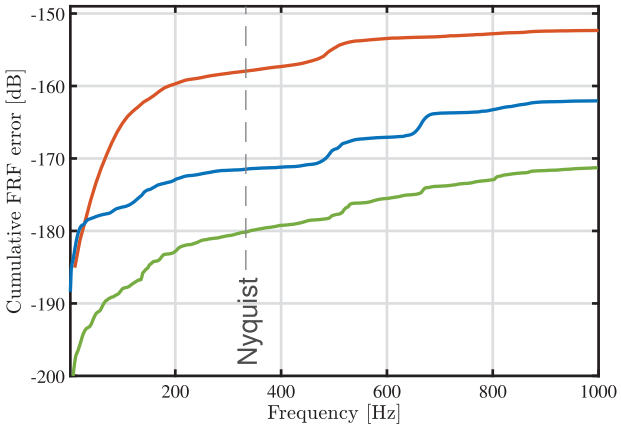

Fig. 7. Developed LRM method (—) achieves the lowest cumulative FRF error from (49) for $G_z(\Omega_k)$ compared to the LPM method from [26] (—) and the SA method (48) (—).

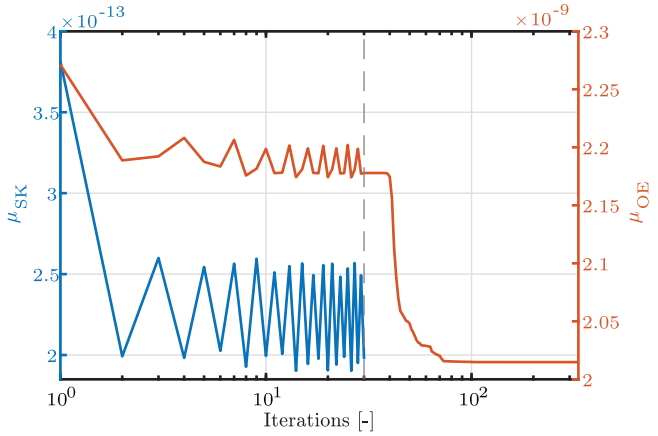

Fig. 8. Mean SK (—) (left axis) and mean least-squares cost (—) from (50) when estimating G_{y_4} (right axis). After 30 SK iterations (– –), additional 300 iterations are done based on the LM algorithm per frequency.

the FRF over 11 segments of the data as

$$\widehat{G}_{\mathrm{SA}}\left(\Omega_p\right) = \frac{\sum_{i=1}^{11} \widehat{Y}_{h,i}\left(\Omega_p\right) \overline{U}_{h,i}\left(\Omega_p\right)}{\sum_{i=1}^{11} U_{h,i}\left(\Omega_p\right) \overline{U}_{h,i}\left(\Omega_p\right)} \quad \forall p \in \{0, 6, 12, \ldots\}, \tag{48}$$

where X_i is the DFT of the i^{th} segment of X, multiplied with a Hanning window, where each segment contains 200 samples with 100 samples' overlap. For validation purposes, the outputs z_l and $\mathcal{S}_d y_4$ are recorded at the fast sampling rate as well, i.e., z_h and y_4 are available. In particular, a validation FRF is constructed using these signals, $N = 50\,000$ samples, and the LRM method from [13], with rational degrees $R_n = R_d = R_m = 4$ and a window size of $n_w = 150$, which is considered to be the ground-truth FRF. The cumulative FRF error for the first n frequencies is defined as

$$\frac{1}{N}\sum_{k=1}^{n}\left|G\left(\Omega_k\right) - \widehat{G}\left(\Omega_k\right)\right|. \tag{49}$$

B. Experimental Results

The true and estimated FRFs of G_{z_4} and G_y are shown in Figs. 5 and 6, with the cumulative error (49) of G_y in Fig. 7. The following observations are made.

1) From the FRFs of G_{y_4} and G_z in, respectively, Figs. 5 and 6, the following is observed.
   a) The developed method $\widehat{G}_{\mathrm{LRM}}$ estimates FRFs G_{y_4} and G_z accurately, even beyond the Nyquist frequency and including resonances and antiresonances.
      i) The deviations around 650–690 and 800–840 Hz occur due to a low "signal-to-signal" ratio. To disentangle aliased contributions, the FRF at these frequencies is estimated jointly with significantly higher gains around 0 Hz and the resonant behavior at 490–530 Hz, which dominate the slow-rate output Y_l compared to the gains at 650–690 and 800–840 Hz.
   b) The LPM method $\widehat{G}_{\mathrm{LPM}}$ estimates the FRFs of G_{y_4} and G_z adequately. However, the lightly damped resonant dynamics are not captured accurately due to the polynomial model structure.
   c) The SA method $\widehat{G}_{\mathrm{SA}}$ estimates the FRFs G_{y_4} and G_z poorly; resonances and antiresonances are modeled incorrectly, specifically above the Nyquist frequency. In addition, the frequency resolution is a factor of 6 lower compared to the LPM and LRM methods.
   d) The developed LRM method results in a significantly lower standard deviation compared to the LPM approach, particularly around resonances and their aliased frequencies. This is expected, as rational models are more suitable for lightly damped resonant dynamics.
2) Fig. 7 clearly shows that the LRM method achieves the lowest cumulative error of G_z.

The observations show that the LRM method is most suitable for identifying fast-rate FRFs of (lightly damped) systems using slow-rate outputs. The LRM method is effective because it disentangles the aliased components through local models, and the rational model structure is capable of estimating the (lightly damped) resonant dynamics accurately.

C. Iterative Analysis

The iterative reweighted solutions described in Section IV-C are analyzed for experimental validation. The mean SK cost and mean least-squares cost for all frequencies are defined as

$$\mu_{\mathrm{SK}} = \frac{1}{N}\sum_{k=0}^{N-1} J_{\mathrm{SK}}\left(\widetilde{\Theta}(k)\right),$$
$$\mu_{\mathrm{OE}} = \frac{1}{N}\sum_{k=0}^{N-1} J_{\mathrm{LS}}\left(\widetilde{\Theta}(k)\right), \tag{50}$$

where J_{SK} and J_{LS} are calculated with (41) and (19), with estimated output $\widehat{Y}_l$ from (14). The mean SK and least-squares

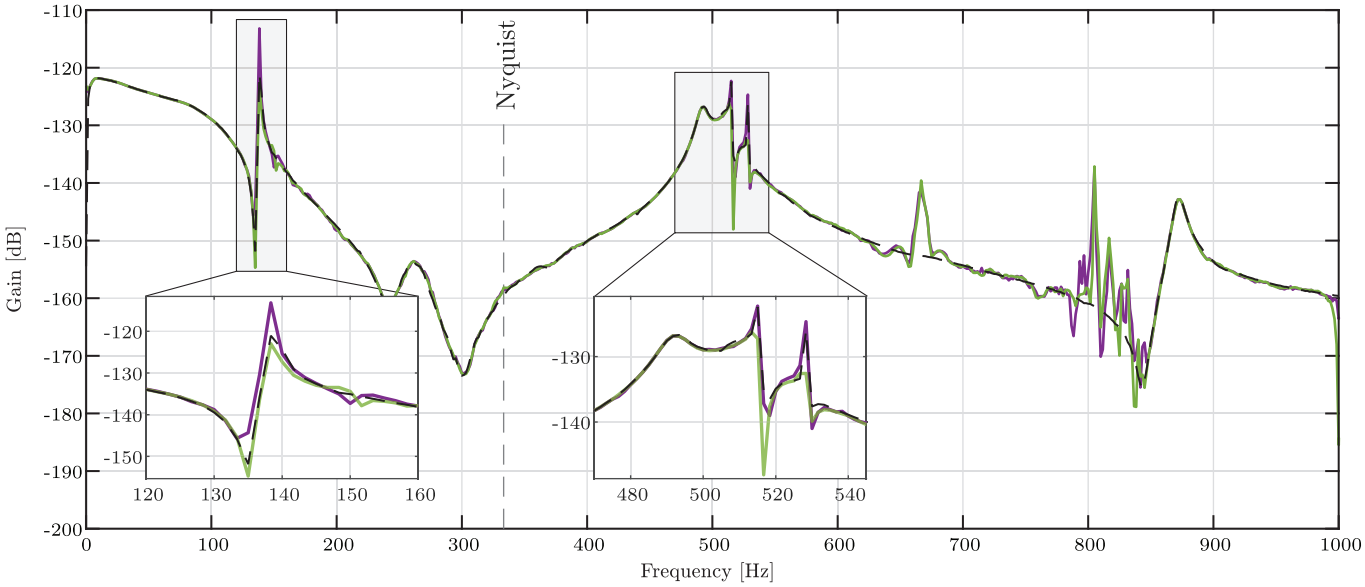

Fig. 9. FRF determined with closed-form solution (32) (—) and the FRF after 30 SK and 300 LM iterations (—) both identify the true FRF $G_{y_4}(\Omega_k)$ (- -) accurately.

cost and the FRF after 30 SK and 300 LM iterations are shown in Figs. 8 and 9.

The following observations are made with respect to the iterative reweighting of the experimental FRF.

1) Both the mean SK and mean least-squares cost in Fig. 8 are decreasing, as expected.
2) After iterative reweighting, the resonant behavior around 500 Hz is estimated slightly more accurate compared to the closed-form solution, as observed from Fig. 9.
3) The mean least-squares cost in Fig. 8 decreases by almost 12% after 30 SK and 300 LM iterations. On the other hand, the FRF after 30 SK and 300 LM iterations in Fig. 9 shows no significant difference compared to the FRF of the closed-form solution, indicating that iterative reweighting is not strictly necessary.

It is concluded that the weighted linear least-squares (21) is suitable for identifying fast-rate FRFs beyond the Nyquist frequency of a slow-rate output of the OAT. This can be explained because weighting the cost function only has a minor effect in the local windows, which was also observed in [14].

VI. Conclusion

The results in this article enable the identification of fast-rate FRFs where aliasing occurs due to slow-rate outputs. The key idea is to parameterize the system and transient FRFs through multiple local rational models, which allows to appropriately disentangle aliased contributions when exciting the full frequency spectrum. The local rational models are effective in modeling rational systems, especially with lightly damped resonant dynamics. A linear least-squares criterion with a unique closed-form solution is determined by appropriately weighting the associated nonlinear cost function. The closed-form solution does not suffer from local minima, in contrast to nonlinear optimization, and additionally enables estimating the variance of the identified FRF. Furthermore, the estimation accuracy of the weighted linear least-squares is improved by means of iterative reweighted solutions, including the Sanathanan-Koerner algorithm. Finally, the framework is validated through experiments on a prototype wafer stage, demonstrating accurate identification of lightly damped resonant dynamics beyond the Nyquist frequency. The developed approach plays a crucial role in the identification and control design of closed-loop, multivariable, and parametric systems, especially for systems with slow-rate outputs, such as vision-in-the-loop systems.

Acknowledgment

The authors would like to thank Leonid Mirkin for his help and fruitful discussions that led to the results of this article.

References

[1] T. Atsumi, "Disturbance suppression beyond Nyquist frequency in hard disk drives," *Mechatronics*, vol. 20, no. 1, pp. 67–73, Feb. 2010.
[2] S. Hutchinson, G. D. Hager, and P. I. Corke, "A tutorial on visual servo control," *IEEE Trans. Robot. Autom.*, vol. 12, no. 5, pp. 651–670, Oct. 1996.
[3] C. Shannon, "Communication in the presence of noise," *Proc. IRE*, vol. 37, no. 1, pp. 10–21, 1949.
[4] M. Mae, W. Ohnishi, and H. Fujimoto, "Multirate feedforward control with mode decomposition for intersample performance in multivariable motion systems," *Control Eng. Pract.*, vol. 141, Dec. 2023, Art. no. 105694.
[5] T. Oomen, M. van de Wal, and O. Bosgra, "Design framework for high-performance optimal sampled-data control with application to a wafer stage," *Int. J. Control*, vol. 80, no. 6, pp. 919–934, 2007.
[6] R. M. Schmidt, G. Schitter, A. Rankers, and J. van Eijk, *The Design of High Performance Mechatronics*. Delft, The Netherlands: Delft Univ. Press, 2020.
[7] R. Pintelon, P. Guillaume, Y. Rolain, J. Schoukens, and H. Van Hamme, "Parametric identification of transfer functions in the frequency domain—A survey," *IEEE Trans. Autom. Control*, vol. 39, no. 11, pp. 2245–2260, Aug. 1994.
[8] R. Pintelon and J. Schoukens, *System Identification: A Frequency Domain Approach*. Hoboken, NJ, USA: Wiley, 2012.

[9] T. Oomen, "Advanced motion control for precision mechatronics: Control, identification, and learning of complex systems," *IEEJ J. Ind. Appl.*, vol. 7, no. 2, pp. 127–140, 2018.
[10] S. Skogestad and I. Postlethwaite, *Multivariable FeedBack Control–Analysis and Design*. Hoboken, NJ, USA: Wiley, 2005.
[11] J. Schoukens, G. Vandersteen, K. Barbé, and R. Pintelon, "Nonparametric preprocessing in system identification: A powerful tool," *Eur. J. Control*, vol. 15, nos. 3–4, pp. 260–274, Jan. 2009.
[12] R. Pintelon, J. Schoukens, G. Vandersteen, and K. Barbé, "Estimation of nonparametric noise and FRF models for multivariable systems—Part I: Theory," *Mech. Syst. Signal Process.*, vol. 24, no. 3, pp. 573–595, Apr. 2010.
[13] T. McKelvey and G. Guérin, "Non-parametric frequency response estimation using a local rational model," in *Proc. 16th IFAC Symp. Syst. Identificat.*, vol. 45, Jul. 2012, pp. 49–54.
[14] R. Voorhoeve, A. van der Maas, and T. Oomen, "Non-parametric identification of multivariable systems: A local rational modeling approach with application to a vibration isolation benchmark," *Mech. Syst. Signal Process.*, vol. 105, pp. 129–152, May 2018.
[15] E. Geerardyn, "User-friendly system identification," Ph.D. dissertation, Vrije Universiteit Brussel, 2016.
[16] K. J. Åström and B. Wittenmark, *Computer-Controlled Systems: Theory Design*. New York, NY, USA: Dover, 2011.
[17] H. Unbehauen and G. P. Rao, "Continuous-time approaches to system identification—A survey," *Automatica*, vol. 26, no. 1, pp. 23–35, Jan. 1990.
[18] L. Ljung, "Experiments with identification of continuous time models," in *Proc. 15th IFAC Symp. Syst. Identif.*, vol. 42. Saint Malo, France, 2009, pp. 1175–1180.
[19] R. Ehrlich, C. Taussig, and D. Abramovitch, "Identification of sampled data systems at frequencies beyond the Nyquist rate," in *Proc. 28th IEEE Conf. Decis. Control*, Dec. 1989, pp. 646–652.
[20] F. Ding and T. Chen, "Identification of dual-rate systems based on finite impulse response models," *Int. J. Robust Nonlinear Control*, vol. 18, no. 7, pp. 589–598, 2004.
[21] J. Ding and F. Ding, "The residual based extended least squares identification method for dual-rate systems," *Comput. Math. With Appl.*, vol. 56, no. 6, pp. 1479–1487, Sep. 2008.
[22] J. Ding, F. Ding, X. P. Liu, and G. Liu, "Hierarchical least squares identification for linear SISO systems with dual-rate sampled-data," *Trans. Autom. Control*, vol. 56, no. 11, pp. 2677–2683, 2011.
[23] Y. Zhu, H. Telkamp, J. Wang, and Q. Fu, "System identification using slow and irregular output samples," *J. Process Control*, vol. 19, no. 1, pp. 58–67, 2009.
[24] D. Li, S. L. Shah, and T. Chen, "Identification of fast-rate models from multirate data," *Int. J. Control*, vol. 74, no. 7, pp. 680–689, 2001.
[25] F. Ding and T. Chen, "Hierarchical identification of lifted state-space models for general dual-rate systems," *IEEE Trans. Circuits Syst. I, Reg. Papers*, vol. 52, no. 6, pp. 1179–1187, Jun. 2005.
[26] M. van Haren, L. Mirkin, L. Blanken, and T. Oomen, "Beyond Nyquist in frequency response function identification: Applied to slow-sampled systems," *IEEE Control Syst. Lett.*, vol. 7, pp. 2131–2136, 2023.
[27] T. Oomen, E. Grassens, and F. Hendriks, "Inferential motion control: Identification and robust control framework for positioning an unmeasurable point of interest," *IEEE Trans. Control Syst. Technol.*, vol. 23, no. 4, pp. 1602–1610, Jul. 2015.
[28] M. F. Heertjes et al., "Control of wafer scanners: Methods and developments," in *Proc. Amer. Control Conf. (ACC)*, Jul. 2020, pp. 3686–3703.
[29] P. Vaidyanathan, *Multirate Systems and Filter Banks*. Upper Saddle River, NJ, USA: Prentice-Hall, 1993.
[30] D. Peumans, R. Pintelon, J. Lataire, and G. Vandersteen, "Frequency response function measurements of multivariable systems via local rational modeling," *IEEE Trans. Instrum. Meas.*, vol. 70, pp. 1–9, 2021.
[31] D. Verbeke and J. Schoukens, "Frequency response measurements with local parametric modeling," *IEEE Trans. Instrum. Meas.*, vol. 69, no. 6, pp. 3249–3261, Jun. 2020.
[32] C. Sanathanan and J. Koerner, "Transfer function synthesis as a ratio of two complex polynomials," *IEEE Trans. Autom. Control*, vol. AC-8, no. 1, pp. 56–58, Jan. 1963.
[33] J. Friedman and P. P. Khargonekar, "A comparative applications study of frequency domain identification techniques," in *Proc. Amer. Control Conf.*, vol. 5, Aug. 2005, pp. 3055–3059.

Max van Haren received the M.Sc. degree (cum laude) in mechanical engineering from Eindhoven University of Technology, Eindhoven, The Netherlands, in 2021, where he is currently pursuing the Ph.D. degree in mechanical engineering with the Control Systems Technology Section.

His research interests include the control and identification of mechatronic systems, including sampled data, multirate, and linear parameter-varying systems.

Lennart Blanken received the M.Sc. and Ph.D. degrees (cum laude) in mechanical engineering from Eindhoven University of Technology, Eindhoven, The Netherlands, in 2015 and 2019, respectively.

He is currently a System Designer in mechatronics with Sioux Technologies, Eindhoven. In addition, he is an Assistant Professor with the Department of Mechanical Engineering, Eindhoven University of Technology. His research interests include advanced feedforward control, learning control, repetitive control, and their applications to mechatronic systems.

Koen Classens (Graduate Student Member, IEEE) received the M.Sc. degree (cum laude) in systems and control and the M.Sc. degree (cum laude) in mechanical engineering from Eindhoven University of Technology, Eindhoven, The Netherlands, in 2019, and the Ph.D. degree from Eindhoven University of Technology, in 2024.

His research interests include control and fault diagnosis for complex high-precision mechatronic systems.

Dr. Classens is a recipient of the Unilever Research Prize.

Tom Oomen (Senior Member, IEEE) received the M.Sc. and Ph.D. degrees (cum laude) from Eindhoven University of Technology, Eindhoven, The Netherlands, in 2005 and 2010, respectively.

He held visiting positions at KTH, Stockholm, Sweden, and the University of Newcastle, Callaghan, NSW, Australia. He is a Full Professor with the Department of Mechanical Engineering, Eindhoven University of Technology. He is also a part-time Full Professor with Delft University of Technology, Delft, The Netherlands. His research interests include data-driven modeling, learning, and control, with applications in precision mechatronics.

Dr. Oomen is a member of Eindhoven Young Academy of Engineering. He was a recipient of the 7th Grand Nagamori Award, the Corus Young Talent Graduation Award, the IFAC 2019 TC 4.2 Mechatronics Young Research Award, the 2015 IEEE Transactions on Control Systems Technology Outstanding Paper Award, the 2017 IFAC Mechatronics Best Paper Award, the 2019 IEEJ Journal of Industry Applications Best Paper Award, and the Veni and Vidi Personal Grant. He has been the Vice-Chair of IFAC TC 4.2. He served on the Editorial Board for IEEE TRANSACTIONS ON CONTROL SYSTEMS TECHNOLOGY. He is currently a Senior Editor of IEEE CONTROL SYSTEMS LETTERS (L-CSS) and the Co-Editor-in-Chief of *IFAC Mechatronics*.